

Reduced order modeling for contaminant transport and mixing in building systems: A case study using dynamical systems techniques

Amit Surana, Nathan Hariharan, Satish Narayanan and Andrzej Banaszuk
United Technologies Research Center
411 Silver Lane
East Hartford, CT 06108

Abstract—In this paper we propose a Lagrangian Coherent Structures (LCS) based approach to modeling and estimation of contaminant transport and mixing in large indoor spaces in buildings. Specifically, we show how the knowledge of LCS can be exploited to enhance Proper Orthogonal Decomposition (POD) based model reduction, sensor placement and comparing effect of different control schemes. We illustrate this approach in a three-dimensional room equipped with a mechanical ventilation system.

I. INTRODUCTION

Increasingly, substantial research efforts are underway to create high performance and energy efficient buildings that meet or exceed the occupant comfort and safety needs at lower life cycle costs and resource utilization. Real-time knowledge of dynamic indoor environment parameters, such as thermal and airflow state, and contaminant distribution are critical to the management and optimization of building occupant comfort and safety. However, the multi-scale spatiotemporal flow dynamics associated with buildings makes the problem of estimation, optimization and control challenging. The key issue in such applications is the lack of rigorous methods for extracting reduced-order model that captures the essential coupling across spatial and temporal scales, and for selecting sensor and actuator placement that enable cost performance trade off's for practical design problems. Solving such problems require a tight integration of IT systems (including sensors, algorithms, computational architecture, and communications) with control, and dynamics.

In this paper we focus on dynamic modeling of transport and mixing of passive contaminant in large indoor spaces in buildings. For such spaces, lumped models like *multizone models* [1] with well-mixed assumptions are inadequate, while CFD models are not directly amenable for real-time monitoring and control. Thus one has to rely on appropriate reduced-order models which can capture the inhomogeneous spatio-temporal dynamics in real time by utilizing information from a limited number of sensors.

One of the most widespread techniques for model reduction in fluids has been Proper Orthogonal Decomposition and Galerkin projection [2], [3]. The central idea of POD is to determine a set of empirical mode shapes, that optimally span the simulation data. Galerkin projection determines the reduced order dynamics, by orthogonal projection of the governing equation on the mode shapes. In this framework the state estimation problem is reduced to estimating a finite

number of Galerkin coefficients. However, an appropriate choice of modes and sensor location is critical to ensure that the resulting estimation algorithm is stable and efficient in predicting the dynamical features of interest. In practice, limited availability of sensors and restriction on their placement due to lack of accessibility and viability, makes the estimation problem even more challenging.

As described above, POD based model reduction is achieved by retaining only those flow modes which capture a large enough proportion of the net energy. However, it is not clear as to how efficiently these energetic modes capture passive contaminant transport and mixing. In order to address this issue we propose a new Lagrangian Coherent Structure (LCS) based metric for choosing POD modes. It is well known that LCS act as templates of transport and mixing in fluid flows [4],[5]. While hyperbolic LCS enhance mixing by causing material stretching, folding and filamentation; the vortical structures trap material and therefore, inhibit mixing. LCS based metric allows one to choose those POD modes that can capture relevant mixing scales. Through a case study, we show that this approach indeed leads to lower order models with fewer number of states as compared to that obtained from an energy based norm. We also demonstrate other applications of LCS, such as in sensor placement for robust estimation, and in analyzing the effect of different actuation schemes, such as forced ventilation and heating, on mixing and transport.

This paper is organized into four sections. In section II we compare Eulerian Coherent Structure and LCS based techniques for extracting coherent structures in three dimensional time dependent fluid flows. LCS based techniques offer several advantages over ECS based ones and are used subsequently in this paper to highlight mixing templates. We describe two such criterion in section III: Direct Lyapunov Exponent (DLE) and M_Z , which can be used to partition the flow domain into hyperbolic and vortex regions. In section IV we demonstrate the role of LCS in model reduction, estimation and control through a case study of airflow and thermal transport in a three dimensional room equipped with a mechanical ventilation system. Finally, in section V we conclude with recommendations for future research.

II. COHERENT STRUCTURES IN THREE DIMENSIONAL TIME DEPENDENT FLOWS

Understanding transport process in fluids requires partitioning of flow domain into regions with different dynamical behaviors [5]. Such dynamical regions are known as *coherent structures*. Accurate identification of the location and nature of these structures and their interaction with each other is fundamental to understanding mixing in fluid flows.

Consider a three dimensional time-dependent velocity field

$$\mathbf{v}(\mathbf{x}, t) = (u(x, y, z, t), v(x, y, z, t), w(x, y, z, t))^T, \quad (1)$$

which describes a fluid flow in domain $\mathbf{D} \subset \mathbb{R}^3$ of interest. The velocity field could represent a solution of the Navier-Stokes equation, is obtained from a flow model or is measured experimentally. Techniques for defining and extracting coherent structures broadly fall into two categories: *Eulerian* and *Lagrangian*. The Eulerian coherent structures (ECS) criteria are typically formulated in terms of the instantaneous velocity field and its gradient. For example, the Okubo-Weiss [6] criterion partitions the domain into vortex and strain regions according to the spatial distribution of the quantity

$$Q = \frac{1}{2}(\|\boldsymbol{\Omega}\|^2 - \|\mathbf{S}\|^2), \quad (2)$$

where, $\|\cdot\|$ is the Euclidean matrix norm,

$$\mathbf{S} = \frac{1}{2}(\nabla\mathbf{v} + \nabla\mathbf{v}^T), \quad \boldsymbol{\Omega} = \frac{1}{2}(\nabla\mathbf{v} - \nabla\mathbf{v}^T), \quad (3)$$

denote the rate of strain tensor and the vorticity field, respectively. Vortex cores are identified with regions where $Q > 0$ and region of strain and deformation are characterized by $Q < 0$. A survey of other such Eulerian criteria, is given in [7], which also reveal various shortcomings of such criteria.

By contrast Lagrangian methods identify flow structures based on the properties of fluid trajectories. Recall that a fluid trajectory $\mathbf{x}(t) = \mathbf{x}(t, t_0, \mathbf{x}_0)$ starting from $\mathbf{x}(t_0, t_0, \mathbf{x}_0) = \mathbf{x}_0$, satisfies the Lagrange equations of particle motion

$$\dot{\mathbf{x}} = \mathbf{v}(\mathbf{x}(t, t_0, \mathbf{x}_0), t). \quad (4)$$

From the viewpoint of geometric theory of dynamical systems, the phase space of (4), is actually the physical space in which the fluid flow takes place. Evidently, “structures” in the phase space of (4) should have some influence on the transport and mixing properties of flow. This realization has lead to plethora of work on applying dynamical systems techniques to the study of transport issues in fluids over the past two decades [4],[5].

Within this dynamical systems framework, the impact of hyperbolic and elliptic structures on mixing in steady, periodic and near-integrable flows has been thoroughly studied. For these restricted classes of flows, the stable and unstable manifolds associated with saddle type fixed points of the velocity field in steady flows or of associated Poincare map for periodic and quasiperiodic flows form global templates of mixing. Unstable manifolds act as attracting material lines

(surfaces) that create global folding patterns for passive tracers; stable manifolds act as repelling material lines (surfaces) that are responsible for stretching of fluid blobs. On the other hand elliptic structures like KAM tori are examples of complete barriers to transport, fluid trajectories starting inside them remain trapped inside forever.

Recent progress in nonlinear dynamics has extended the above picture to velocity fields with aperiodic or even turbulent time dependence. While no Poincare maps are available in this context, families of hyperbolic material lines and surfaces continue to organize passive mixing. These families are formed by *finite-time* stable and unstable manifold of distinguished fluid trajectories [7], [9]-[12]. In next section we describe two Lagrangian criteria which have duality property, i.e. can be used to detect vortex cores and the hyperbolic skeleton simultaneously in 3D aperiodic velocity fields. Before we proceed further, two remarks are in order:

- (1) Neglecting molecular diffusion, passive scalars (e.g. dye, temperature, CO_2 , SO_6 or any material that can be considered to have negligible effect on the flow) also follow the fluid trajectories. Transport of contaminants with finite volume like smoke is significantly more challenging problem and is beyond the scope of this paper. For recent development in this direction, we refer the reader to [13].
- (2) Despite additional computational cost, the Lagrangian methods in general offer several advantages over Eulerian techniques: they lead to consistent and accurate description of mixing templates in unsteady flows [9]-[12], these methods are objective i.e. frame-independent [7], insensitive to short-term anomalies in the velocity field [9], have the ability to define structure boundaries with greater details and most significantly do not rely on preselected threshold [8].

III. TOOLS FOR DETECTING LCS

A. Direct Lyapunov Exponent

The Direct Lyapunov Exponent (DLE) is a scalar field which at each point measures the rate of separation of neighboring particle trajectories initialized near the point. In the Lagrangian frame, an infinitesimal perturbation ξ to the initial condition \mathbf{x}_0 is advected by the linearized flow

$$\dot{\xi} = \nabla\mathbf{v}(\mathbf{x}(t), t)\xi, \quad (5)$$

the equation of variation associated with the trajectory $\mathbf{x}(t)$. Recall that the fundamental matrix solution of the linear time-dependent system (5) is the deformation gradient $\nabla_{\mathbf{x}_0}\mathbf{x}(t, t_0, \mathbf{x}_0)$. Thus, the coefficient of particle separation is determined by the largest singular value of $\nabla_{\mathbf{x}_0}\mathbf{x}(t, t_0, \mathbf{x}_0)$, i.e.

$$\Lambda_{\max}(t, t_0, \mathbf{x}_0) = \lambda_{\max}(\nabla_{\mathbf{x}_0}\mathbf{x}(t, t_0, \mathbf{x}_0)^T \nabla_{\mathbf{x}_0}\mathbf{x}(t, t_0, \mathbf{x}_0)). \quad (6)$$

The DLE field is then defined as [12], [15], [16]

$$\sigma_{t_0}^t(\mathbf{x}_0) = \frac{1}{2|t - t_0|} \ln \Lambda_{\max}(t, t_0, \mathbf{x}_0). \quad (7)$$

Since the maximum eigenvalue is used in the definition of $\Lambda_{\max}(t, t_0, \mathbf{x}_0)$, direction information is not retained in $\sigma_{t_0}^t(\mathbf{x}_0)$. A point \mathbf{x}_0 will have a high DLE value if there is a great amount of expansion in one direction, even if there is compression in all other directions.

Regions of maximal stretching generates a local maximizing surface (ridge) for the DLE field. For an appropriate choice of integration time $T > 0$ repelling LCS at t_0 can be located as ridges of the $\sigma_{t_0}^{t_0+T}(\mathbf{x}_0)$ field. Similarly attracting LCS at t_0 can be located as ridges of the $\sigma_{t_0}^{t_0-T}(\mathbf{x}_0)$. Consideration for time scales of the flow and numerical experimentation is usually sufficient to determine an appropriate time scale T [17]. For most practical purposes, however, the primary topological features of the LCS extracted from the DLE field are insensitive to the integration time T .

While maximal stretching generates ridges for the DLE field, the converse is not true: local maxima of the DLE field may indicate either locally maximal stretching or locally maximal shear. In order to confirm that the ridges are indeed hyperbolic LCS, instead of regions of maximal shear, one may calculate the strain rate normal to the ridge as discussed in [14]. DLE technique is not always well suited to locate vortices; the primary reason being that, both vortical regions and parallel shear lead to relatively low values in the DLE field. In next section we describe another criteria which can be used to identify vortices unambiguously in incompressible flows.

B. M_Z Criterion

Haller [7], recently derived an objective i.e. frame independent criteria to detect vortices as regions of Lagrangian stirring. This approach is based on partitioning the fluid domain into hyperbolic and elliptic regions, by examining the behavior of the quadratic form $\langle \xi, \mathbf{M}(\mathbf{x}(t), t)\xi \rangle$, on the zero strain cone Z

$$Z = \{\xi | \langle \xi, \mathbf{S}(\mathbf{x}, t)\xi \rangle = 0\}. \quad (8)$$

where, \mathbf{S} is given by Eq. (3), ξ is the perturbation in Eq. (5) and $\langle \cdot, \cdot \rangle$ is the standard inner product on \mathbb{R}^3 and

$$\mathbf{M} = \partial_t \mathbf{S} + \nabla \mathbf{S} \mathbf{v} + \mathbf{S} \nabla \mathbf{v} + (\nabla \mathbf{v})^T \mathbf{S}, \quad (9)$$

is the strain acceleration tensor. It turns out that restriction of $\langle \xi, \mathbf{M}(\mathbf{x}(t), t)\xi \rangle$ to Z , which we denote by M_Z is either positive definite or indefinite at a generic point. As result fluid domain can be partitioned into two complementary regions

- 1 Hyperbolic domain $\mathcal{H}(t)$, where M_Z is positive definite. It turns out that the fluid trajectories in this domain are Lagrangian-Hyperbolic.
- 2 Elliptic Domain $\mathcal{E}(t)$, where M_Z is indefinite. Physically in this domain the material elements do not align with subspaces that are near the positive eigenspaces of the rate of strain, leading to Lagrangian stirring.

Based on this partition, Haller defines a vortex to be bounded and connected set of fluid trajectories along which M_Z is indefinite. In practice to account for numerical errors,

a more robust M_Z criteria is implemented, according to which a vortex is a set of fluid trajectory along which M_Z is indefinite for much longer times than along nearby trajectories (see [7] for details).

C. Numerical Implementation

In this section we summarize the numerical scheme to compute the DLE field $\sigma_{t_0}^t(\mathbf{x}_0)$ and M_Z criteria over the fluid domain \mathbf{D} .

- (1) Initialize a grid \mathbf{x}_0 of particles at time t_0 in \mathbf{D} .
- (2) Integrate path lines for T seconds. We use a 4th-order Runge-Kutta integration with constant time step. For interpolating velocity field at particle positions we use cubic interpolation in space and linear interpolation in time.
- (3) For each particle trajectory started at (\mathbf{x}_0, t_0) determine the scalar fields $\sigma_{t_0}^t(\mathbf{x}_0)$ and M_Z :
 - a) For finding $\sigma_{t_0}^t(\mathbf{x}_0)$ the deformation gradient is obtained by direct numerical differentiation of particle paths $\mathbf{x}(T+t_0, t_0, \mathbf{x}_0)$ w.r.t. to initial grid \mathbf{x}_0 using finite differencing.
 - b) \mathbf{M} and Z are computed by finite differencing in both space and time.

Following points need to be noted,

- (1) The time scale T for pathline integration is determined by numerical experimentation.
- (2) For particles which reach the boundary $\partial \mathbf{D}$ of the domain \mathbf{D} before time T elapses, pathline integration is stopped. This may result in spurious ridges in the scalar fields which need to be filtered out.
- (3) The ridge extraction from scalar fields can be accomplished using either *height ridges*[18] or *watersheds*[19]. A comparison of these two approaches is given in [19]. In this paper we employ sectional visualization of LCS to demonstrate their role in transport and lower order modeling.

IV. CASE STUDY: 3D ROOM WITH VENTILATION

In this section we demonstrate, how the knowledge of LCS can be exploited for reduced order modeling and estimation of contaminant transport in building systems. For this purpose we consider a room equipped with a mechanical ventilation system as shown in the figure 1. The dimensions of the the room are $[0, x_m] \times [0, y_m] \times [0, z_m]$, where $x_m = 6.2$, $y_m = 2.2$ and $z_m = 2.9$ meters. There are inflow and outflow ducts located on the ceiling and constant temperature heat sources on the floor. By controlling the ventilation and heat inflow, different airflow patterns can be generated in the room.

A. Model reduction

The airflow in the room with no heat inflow is governed by incompressible Navier Stokes equations

$$\frac{\partial \mathbf{v}}{\partial t} = -\mathbf{v} \cdot \nabla \mathbf{v} + \nu \nabla^2 \mathbf{v} - \frac{1}{\rho} \nabla p, \quad (10)$$

$$\nabla \cdot \mathbf{v} = 0, \quad (11)$$

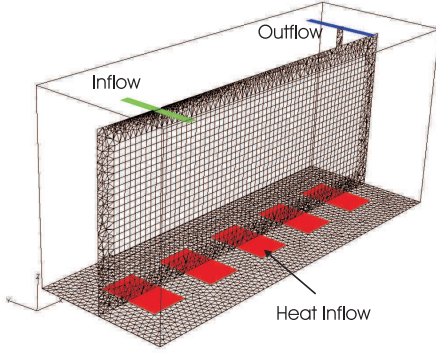


Fig. 1. 3D Room equipped with a mechanical ventilation system

where, p is the pressure, ρ is density and ν is the kinematic viscosity of fluid. The numerical solution is obtained using FLUENT, a commercially available CFD software. We shall denote by $\mathbf{v}_k = \mathbf{v}(\mathbf{x}, t_k)$, snapshots of velocity field at time instants t_k , where $k = 1, \dots, m$.

In snapshot based POD method, the velocity field is expanded as

$$\mathbf{v}(\mathbf{x}, t) = \sum_{i=1}^n a_i(t) \phi_i(\mathbf{x}), \quad (12)$$

where, $n \leq m$ and $\phi_k(\mathbf{x})$, $k = 1, \dots, m$ are spatial modes obtained by solving an eigenvalue problem [3]. Reduced order model is then obtained by Galerkin projection of Navier Stokes equations, which yields a systems of nonlinear ODE's

$$\dot{\mathbf{a}}_k = L_k \mathbf{a} + \mathbf{a}^T Q_k \mathbf{a}, \quad (13)$$

where, $\mathbf{a}(t) = (a_1(t), \dots, a_n(t))^T$, L_k and Q_k are matrices which depend on $\phi_k(\mathbf{x})$, and $k = 1, \dots, n$. The initial conditions $\mathbf{a}(0)$ are generally not known and the value of $\mathbf{a}(t)$ must be replaced by an estimate $\hat{\mathbf{a}}(t)$ to obtain velocity predictions. To obtain an estimate $\hat{\mathbf{a}}(t)$, we employ an Extended Kalman Filter as the nonlinear observer with measurements available from two velocity sensors located at $\mathbf{x}_1 = (0, y_m/2, z_m/2)$ and $\mathbf{x}_2 = (x_m, y_m/2, z_m/2)$. The sensors measure the three components of the velocity field at each location.

Figure 2 shows the estimated velocity field at the sensor locations, using different number of modes. For comparison we also plot the actual velocity field at these locations. Note that with $n = 4$ modes the sensor measurements can be tracked exactly. However, figure 3 shows that $n = 2$ modes can capture 98% of average energy, while for $n = 3, 4$ the average energy reproduced by POD reduces (due to spurious effects of higher order modes). Thus from energy viewpoint first two dominant modes are sufficient to estimate the velocity field well.

In figures 4 and 5 we show the LCS highlighted by backward time DLE field in the mid sections of the room at two different time instants $t_0 = 50$ and $t_0 = 90$. The darker colors indicate higher DLE values, which correspond to intersections of attracting material surfaces with the mid

sections. The subplots (a)-(c), in the first column correspond to LCS computed using CFD data, the subplots (d)-(f) are LCS obtained from estimated velocity field using $n = 1$ mode in POD reduction and the last column (subplots (g)-(i)) being that for $n = 2$ modes. It is evident from these plots, that even though one mode on an average captures only 86% of energy in the simulation data (see Fig. 3) it is able to reproduce the LCS fairly accurately. Note that while at $t_0 = 50$, LCS based on one mode differs slightly (compare subplots (b) and (e) in Fig. 4), but as the estimation of velocity field improves over time, the LCS become more accurate. This study reveals that from contaminant transport viewpoint one mode POD reduction is sufficient, compared to two mode reduction inferred from the energy metric.

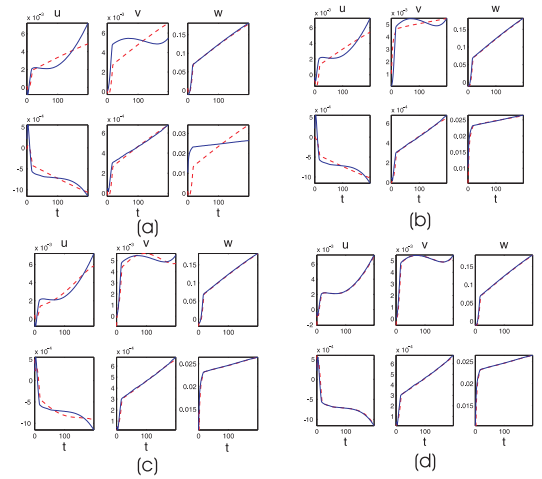


Fig. 2. Comparison of estimated velocity components (dotted red line) with the exact velocity components (solid blue) at the sensor locations. Different subplots correspond to different number of modes used in POD based reconstruction: (a) $n = 1$, (b) $n = 2$, (c) $n = 3$ and (d) $n = 4$.

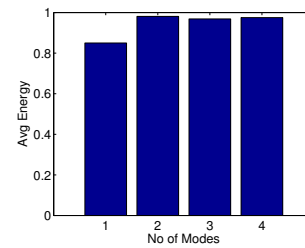


Fig. 3. Time average of energy captured by different number of modes in POD based velocity estimation.

B. Evaluating actuation schemes

In this section we study the effect of heat inflow in addition to forced ventilation on the coherent structures in the room. In order to compute the airflow in this configuration, compressible Navier Stokes equation are solved in FLUENT; for brevity we do not describe the details of the computation.

Heating along with ventilation induces an unsteady airflow in the room. Fig. 6 shows the time evolution of backward time DLE and \mathbf{M}_Z fields in $x = \text{const}$ sections with heating

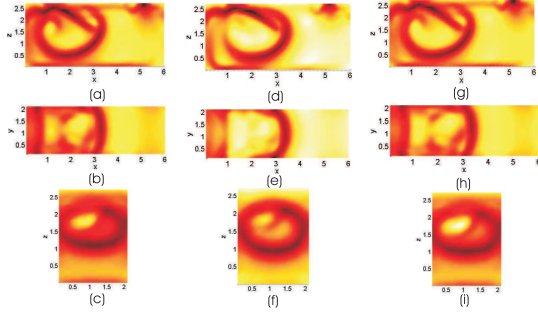


Fig. 4. Comparison of DLE field in mid sections of the 3D room at $t_0 = 50$ sec. Subplots (a)-(c) correspond to backward time DLE field in mid y , z and x sections, respectively. Subplots (d)-(f) are similar LCS plots computed using estimated velocity field with $n = 1$ mode POD. Subplots (g)-(i) are analogous to (d)-(f), but are based on $n = 2$ mode POD reduced order model.

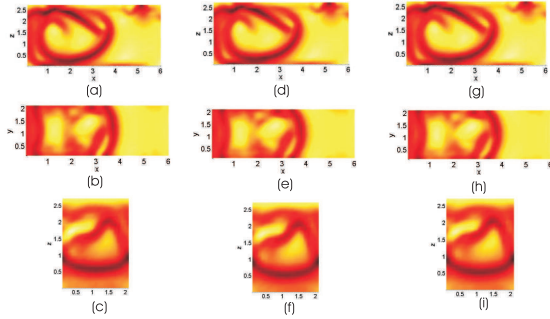


Fig. 5. Same as Figure 4, but for time $t_0 = 90$.

and forced ventilation. In these plots darker colors indicate higher values of the scalar fields; therefore, darker colors in DLE plot correspond to attracting LCS, while darker colors in M_Z plot correspond to vortex regions. It is evident that LCS vary drastically over time. In Fig. 7 we show the DLE in all the mid sections simultaneously, revealing the intricate structure of attracting LCS. Such structures typically arise in flows with chaotic mixing [7].

For comparison we also plot in Fig. 8, the backward time DLE field and M_Z at $t_0 = 50$ sec in the mid sections with only forced ventilation (color coding is same as in Figs. 6,7). Clearly a vortical structure exists in the left half of the room and the airflow is not well mixed. Moreover this structure is stable and does not vary over time. Above analysis, thus reveals that introducing heating destabilizes this vortex and gives rise to a well mixed flow.

C. Sensor placement

In this section we address the problem of number of sensors and their placement that would lead to robust contaminant estimation. A similar problem for optimal placement of sensors in order to detect the largest number of contaminant release scenarios with the minimum number of sensors, was considered in [20]. In this approach, the data recorded from all the possible release scenarios at all possible sensor locations was used to identify the optimal sensor locations.

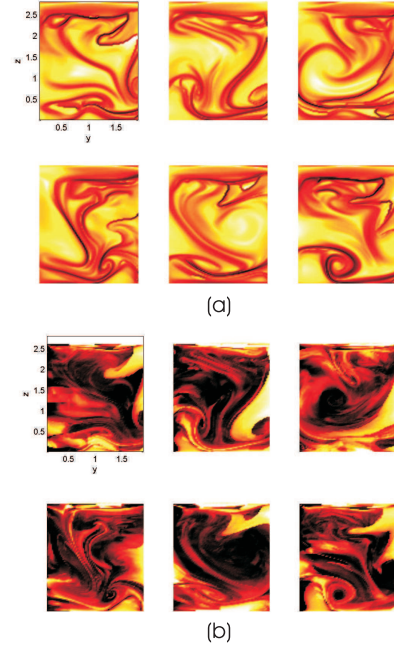


Fig. 6. Snapshots of DLE and M_Z criteria in mid x sections of the room with ventilation and heat inflow at time instants $t_0 = 50, 70, 90, 110, 130, 150$ sec.

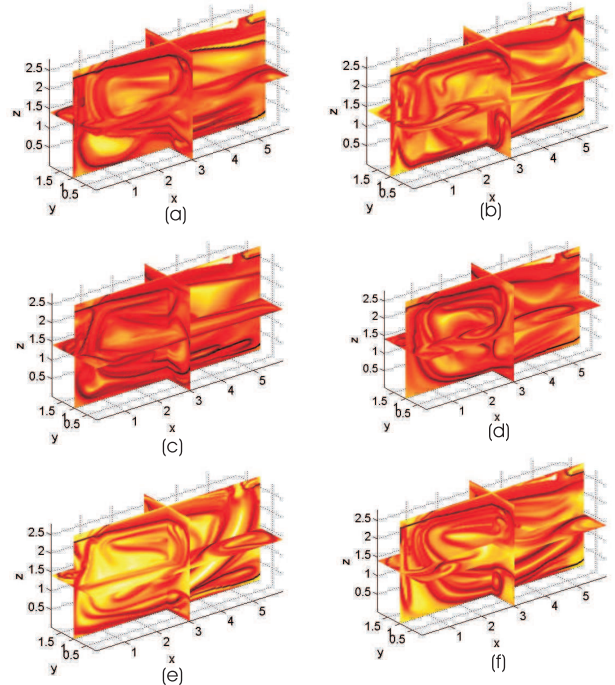


Fig. 7. DLE field in the mid x , y and z sections of the room with ventilation and heating. The subplots correspond to same time instants as in Fig. 6

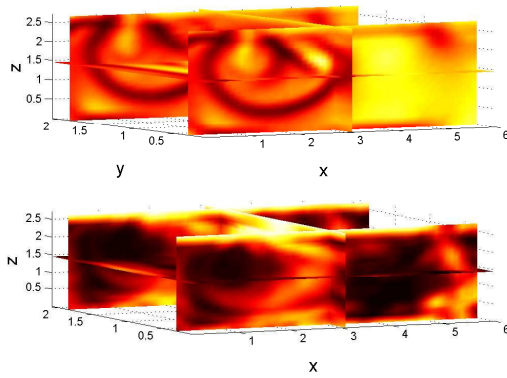


Fig. 8. Backward time DLE and M_z plots at $t_0 = 50$ sec, in the room with only ventilation active. The slices shown correspond to $x = 0.15x_m$, $x = 0.85x_m$, $y = 0.5y_m$ and $z = 0.5z_m$.

Despite the recursive nature of the scheme proposed [20], the technique requires extensive computational effort.

The knowledge of LCS however reveals number of sensors and their locations in a natural fashion. For instance the LCS computation in previous section showed that the room with only forced ventilation, is partitioned into two vortical zones, with no fluid interaction between them. Thus at least two sensors are required at $x = 0$ and $x = x_m$ wall to detect contaminant release which could occur at any location in the room. On the other hand with additional heating the flow becomes chaotic and well mixed. Hence, even one sensor is sufficient to detect contaminant release. With this simple analysis we can conclude that two sensors at two end walls are sufficient to capture contaminant transport in the room which operates under two possible conditions. This approach can be easily generalized to multiple operating scenarios.

V. CONCLUSION AND FUTURE WORK

In this paper we explored a new LCS based metric to be used in conjunction with POD based model-reduction technique for large-scale contaminant transport problem in building environments. This new metric chooses POD modes that capture relevant mixing scales, rather than the modes which retain high percentage of energy contained in simulation data. Application of this metric to airflow in three dimensional room equipped with a mechanical ventilation system, showed that it indeed leads to lower order model, than that based on energy metric. We also showed how knowledge of LCS can guide sensor placement and help develop insights into effects of different actuation schemes on the transport. In particular we found that heat inflow coupled with forced ventilation leads to a well mixed chaotic flow.

Undoubtedly, much room is left for further development. First of all a more quantitative method needs to be devised for LCS comparison and for identifying the relevant modes via projection, rather than relying on visual analysis, adopted in this paper. Compressibility effects become important with heating; the efficacy of LCS based metric needs to

be investigated for POD reduction in compressible flows. Another interesting question is the detection of the location of contaminant source based on the knowledge of LCS. Finally, design of feedback control laws that rely on the reduced order models and manipulate the global LCS through energy efficient micro local actuation [21], remains another challenging issue to be pursued in future.

VI. ACKNOWLEDGMENTS

The funding provided by United Technologies Research Center for this work is greatly appreciated.

REFERENCES

- [1] W. S. Dols, A tool for modeling airflow and contaminant transport, *ASHRAE J.*, March 2001, pp 35-41.
- [2] P. Holmes, J. L. Lumley and G. Berkooz, *Turbulence, Coherent Structures, Dynamical Systems and Symmetry*, Cambridge University Press, 1996.
- [3] C. W. Rowley, Modeling, Simulation, and Control of Cavity Flow Oscillations, Ph. D. Thesis, California Institute of Technology, 2001.
- [4] J. M. Ottino, *The kinematics of mixing, stretching, chaos and transport*, Cambridge Text in Applied Mathematics, Cambridge University Press, 1993.
- [5] S. Wiggins, *Chaotic Transport in Dynamical Systems*, Springer-Verlag, 1993.
- [6] J. C. R. Hunt, A. Wray and P. Moin, Eddies, streams, and convergence zones in turbulent flows, *Center for Turbulence Reserach Report CTR-S88*, 1988.
- [7] G. Haller, An objective definition of a vortex, *J.F.M.*, vol. 525, 2005, pp 1-26.
- [8] M. A. Green, C. W. Rowley and G. Haller, Detection of Lagrangian coherent structures in 3D turbulence, *J.F.M.*, vol. 525, 2005, pp 1-26.
- [9] G. Haller, Finding finite-time invariant manifolds in two-dimensional velocity data, *Chaos*, vol. 10, 2000, pp 99-108.
- [10] G. Haller and G. Yuan, Lagrangian coherent structures and mixing in two-dimensional turbulence, *Physica D*, vol. 147, 2000, pp 352-370.
- [11] G. Haller, Lagrangian coherent structures and the rate of strain in two-dimensional turbulence, *Phys. Fluids A*, vol. 13, 2001, pp 3365-3385.
- [12] G. Haller, Distinguished material surfaces and coherent structures in three-dimensional fluid flows, *Physica D*, vol. 149, 2001, pp 248-277.
- [13] T. Sapsis and G. Haller, Instabilities in the dynamics of neutrally buoyant particles, submitted to *Phys. Fluids*, 2007.
- [14] M. Mathur, G. Haller, T. Peacock, J.E.R. Felsot and H. L. Swinney, Uncovering the Lagrangian skeleton of turbulence, *Physics Review Letters*, vol. 98, 2007 (144502).
- [15] S. C. Shadden, F. Lekien and J. E. Marsden, Definition and properties of Lagrangian coherent structures from finite-time Lyapunov exponent in two-dimensional aperiodic flows, *Physica D*, vol. 212, 2005, pp 271-304.
- [16] F. Lekien, S. C. Shadden and J. E. Marsden, Lagrangian coherent structures in n-dimensional systems, *Journal of Mathematical Physics*, vol. 48, 2007 (065404).
- [17] F. Leiken and N.E. Leonard, "Dynamically consistent Lagrangian coherent structures", *Experimental Chaos: 8th Experimental Chaos Conference*, AIP Conf. Proc 742, 2004, pp 132-139.
- [18] F. Sadlo and R. Peikert, Visualizing Lagrangian coherent structures and comparison to vector field topology, to appear in *Topology based methods in visualization, mathematics+Visualization*, Springer, 2007.
- [19] J. Sahner, T. Weinkauff, N. Teuber and H. Hege, Vortex and strain skeletons in Eulerian and Lagrangian frames, *IEEE Transactions on Visualization and Computer Graphics*, vol. 13(4), 2007, pp 1-10.
- [20] R. Lohner and F. Camelli, Optimal placement of sensors for contaminant detection based on detailed 3D CFD simulations, *International Journal for Computer-Aided Engineering and Software*, vol. 22, 2005, pp 260-273.
- [21] Y. Wang, G. Haller, A. Banaszuk and G. Tadmor, Closed-loop lagrangian separation control in shear flow model, *Phys. Fluids*, vol. 15(8), 2003, pp 2251-2266.